Pergamon

0301-9322(94)00059-X

Int. J. Multiphase Flow Vol. 21, No. 1, pp. 107–117, 1995
Copyright © 1995 Elsevier Science Ltd
Printed in Great Britain. All rights reserved
0301-9322/95 $9.50 + 0.00

AN UPWARD TURBULENT BUBBLY BOUNDARY LAYER ALONG A VERTICAL FLAT PLATE

E. MOURSALI, J. L. MARIÉ and J. BATAILLE

Laboratoire de Mécanique des Fluides et d'Acoustique, URA C.N.R.S. 263, Ecole Centrale de Lyon/Université Claude Bernard Lyon I, ECL BP 163, 69131 Ecully Cedex, France

(Received 30 July 1993; in revised form 20 July 1994)

Abstract—The structure of an upward wall-bounded bubbly flow is investigated in the simple case of a turbulent boundary layer developing on a vertical flat plate. The data reported is part of a research program currently under progress. They concern the void fraction distribution, the wall shear stress, and the mean liquid velocity profiles. It is shown that depending on their mean diameter, a significant fraction of the bubbles deflected towards the wall. This migration, together with a significant deceleration of the bubbles at the surface, prove to be the two main mechanisms responsible for the so-called void peaking phenomenon. Besides, the skin friction coefficient which depends both on the amplitude of the peak, and on the free-stream velocity is found to increase in the presence of the dispersed phase. This increase is linked to a modification of the universal logarithmic law of the wall, and to a depression of the wake.

Key Words: bubbly boundary layer, bubble migration, wall shear stress, modified law of the wall

1. INTRODUCTION

The modelling of gas–liquid bubbly flows requires a reasonably accurate description of the interaction between the bubbles and the liquid phase both in the vicinity of a boundary and in an unbounded domain. The latter was recently studied by co-workers (Lance & Bataille 1991; Lance *et al.* 1991). On the other hand, a number of experiments on pipe flows have already been reported in the literature (Serizawa *et al.* 1975; Michiyoshi & Serizawa 1984; Wang *et al.* 1987; Souhar 1989; Liu & Bankoff 1990). However, they have all been performed in pipes of small diameters, making the measurements and their interpretation quite difficult.

The aim of the present paper is to give the preliminary results of a detailed experimental study of a much simpler configuration, that of a turbulent boundary layer developing on a vertical flat plate immersed in a uniform upward bubbly flow. The experimental facility, the instrumentation techniques, and the characteristics of the upstream flow are described in sections 2, 3 and 4, while the void migration, its dependence on the diameter of the bubbles, the behaviour of the wall shear stress and the mean liquid velocity profiles are investigated in section 5.

2. EXPERIMENTAL FACILITY

A detailed description of the experimental facility can be found in Lance & Bataille (1991). The hydrodynamic tunnel is a closed loop, with a 50 m^3 tap water tank and a 2.5 m long vertical square channel, whose cross section is $400 \times 400\ mm^2$. It is operated in the upward direction at atmospheric pressure, ambient temperature and at liquid velocities U_L which do not exceed 1.5 m/s. Air is blown uniformly into the water, 1 m upstream of the inlet of the test section through an array of 312 stainless steel needles, 0.4 mm i.d., supported by a 40 mm square mesh grid made of cylindrical rods, 8 mm dia. The upstream void fraction thus obtained varies from 0 to 6%, depending on the injection pressure. Within that range, the bubbles whose mean diameter D_B ranges from 3 to 8 mm, are approximately oblate spheroidal, and have a mean velocity U_B given by: $U_B = U_L + U_R$, where the relative velocity U_R is of the order of 20 cm/s. The LDA measurements which were performed in the absence of both the bubbles and the flat plate show that the longitudinal mean velocity of the liquid proves constant to better than 1% and that the intensity of the turbulence generated by the grid remains lower than 2% in the test section.

The plate, which is 15 mm thick, 400 mm wide (Z-direction), and 2 m long (X-direction) is made of Plexiglas. It is located at the center of the test section (see figure 1) and its ogive shaped leading edge lies 0.5 m downstream of the inlet. The transition of the boundary layer is triggered by a rough abrasive ribbon, 3 cm wide, stuck on the surface immediately downstream of the leading edge. Measurements were performed at the following stations along the plate: $X = 0.07$ m, $X = 0.2$ m, $X = 1$ m, $X = 1.5$ m. The intrusive probes are fixed on a rod whose motion in the transverse direction Y is controlled by a motorized micrometer screw device. An optical transducer is used to read their exact position with an accuracy of 10 μm.

3. INSTRUMENTATION

The characterization of the single-phase boundary layer was performed with a standard Laser Doppler Velocimeter composed of a 2.5 W argon laser, a Bragg cell, a frequency shifter and a frequency tracker.

The local skin friction was measured using a hot film, flush-mounted at the surface of the plate, and connected to a constant temperature anemometer. It has been shown by Sandborn (1979) that

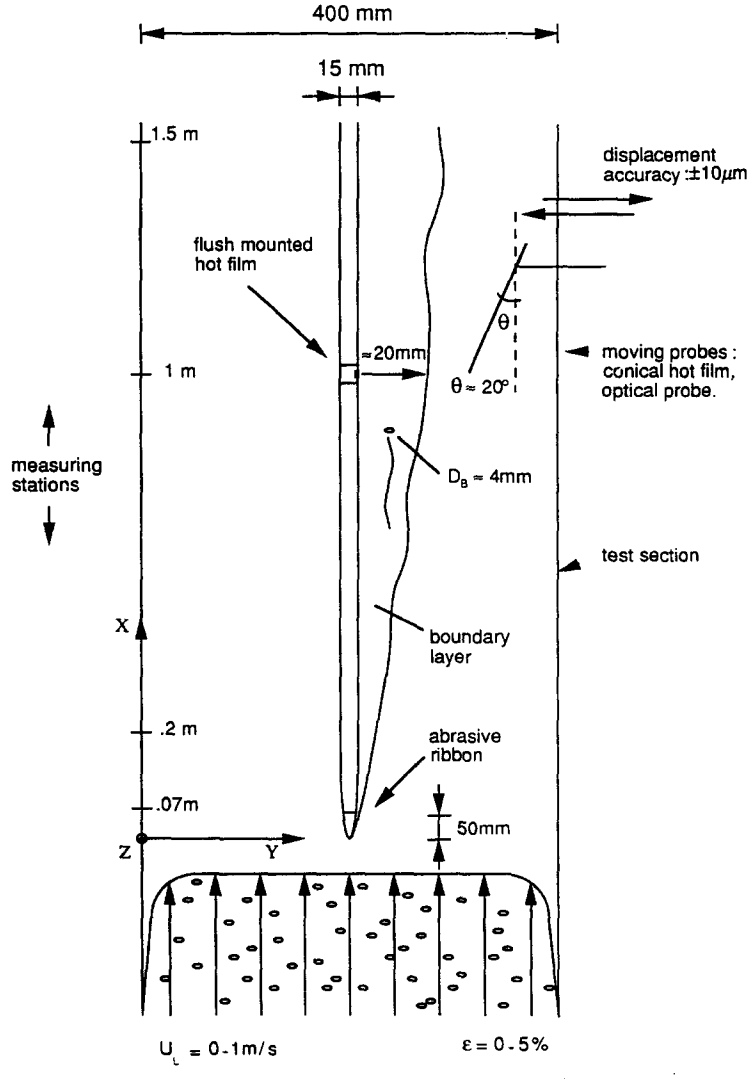

Figure 1. Sketch of the experiment.

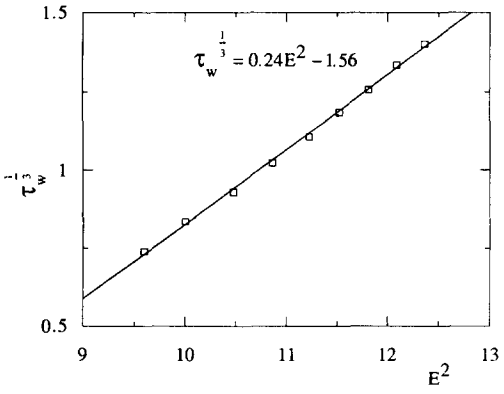

Figure 2. Calibration curve of the flush-mounted hot film

when the film is kept at a constant temperature, the time average wall shear stress (τ_w) in a turbulent steady single-phase boundary layer is related to the mean voltage output (E) by:

$$\tau_w^{\frac{1}{3}} = AE^2 + B \qquad [1]$$

where A and B are two constants to be determined by calibration. The above relationship which is an extension of a formula originally derived by Bellhouse & Schultz (1966) for laminar flows only holds if the thermal boundary layer δ_T is much thinner than the viscous sublayer δ_V and if the voltage fluctuations are negligible. In the absence of bubbles, both conditions are fulfilled. Typically, $\delta_T = 0.5\delta_V$, $e' \leqslant 0.03E$. It is therefore straightforward to determine the single-phase calibration curve shown in figure 2 from the mean skin friction. The latter may either be measured with a Preston tube located 2 cm away from the film in the Z-direction or using the standard theoretical correlation (Schlichting 1968). Both methods agree within 3%. It is assumed that the curve remains valid in bubbly flow and can be used to obtain the two-phase friction coefficient. As a matter of fact, although they increase slightly, the voltage fluctuations remain negligible ($e' \leqslant 0.05E$). Besides, no bubble ever touches the wall (see section 5.1). The uncertainty of the measurements is difficult to evaluate although it is reasonable to believe that the precision is better than 10%.

The local void fraction and bubble frequency were determined with a Photonetics "Optoflow" optical probe consisting of a single, 5 m long optical fiber whose tip had a diameter of 50 μm, which was smaller than the thickness of the viscous sublayer (150 μm), making it possible to investigate the immediate vicinity of the wall. In order to better reach the surface, the probe was inclined at an angle of 20° from the flow direction. The initial distance from the wall was adjusted using a telescope. The zero was taken as the probe came into contact with the plate. The accuracy of such measurements is of the order of 5%.

Finally, the diameters, the shapes and the velocities of individual bubbles were estimated from high speed video films of a plane screen of bubbles ($\approx$3 cm thick) taken with a NAC HSV 200 camera (200 frames/s). In order to generate the screen, the air supply was restricted to just one center line of injectors, parallel to the Y axis, following a procedure previously described by Marié & Lance (1983).

4. CHARACTERISTICS OF THE BASIC FLOW

4.1. Single-phase boundary layer

In the absence of bubbles and for a free-stream velocity U_{LE} of 1 m/s, the thickness of the boundary layer δ, which develops on the flat plate is of the order of 22 mm at a station $X = 1$ m downstream of the leading edge and the associated Reynolds number, R_δ, is of the order of 22,000. Typical mean velocity and turbulent intensity profiles are shown in figure 3. As can be seen in figure 4, in velocity defect form, the experimental data fit the universal logarithmic law

$$\frac{U_{LE} - U_L}{U_*} = -2.44 \ln \frac{Y}{\delta} + 2.35 \qquad [2]$$

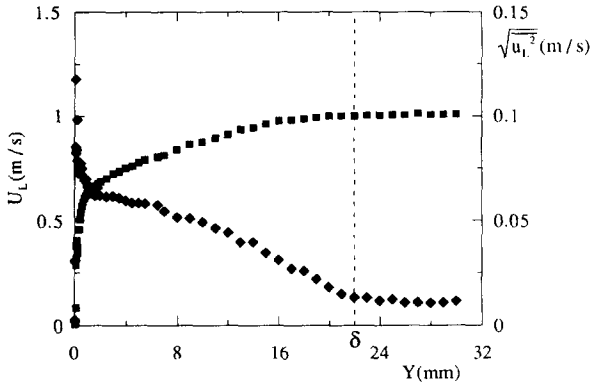

Figure 3. Velocity and longitudinal fluctuation profiles without bubbles. $X = 1$ m; $U_{LE} = 1$ m/s; $\delta = 22$ mm.

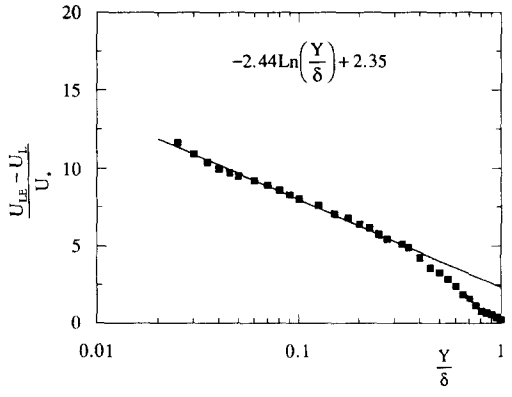

Figure 4. Velocity profile under defect form. X = 1 m.

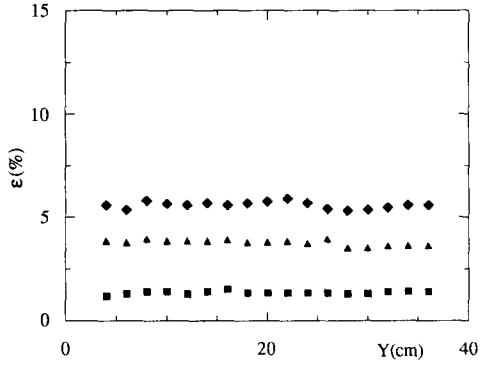

Figure 5. Void fraction profiles upstream of the plate. $U_L = 1$ m/s.

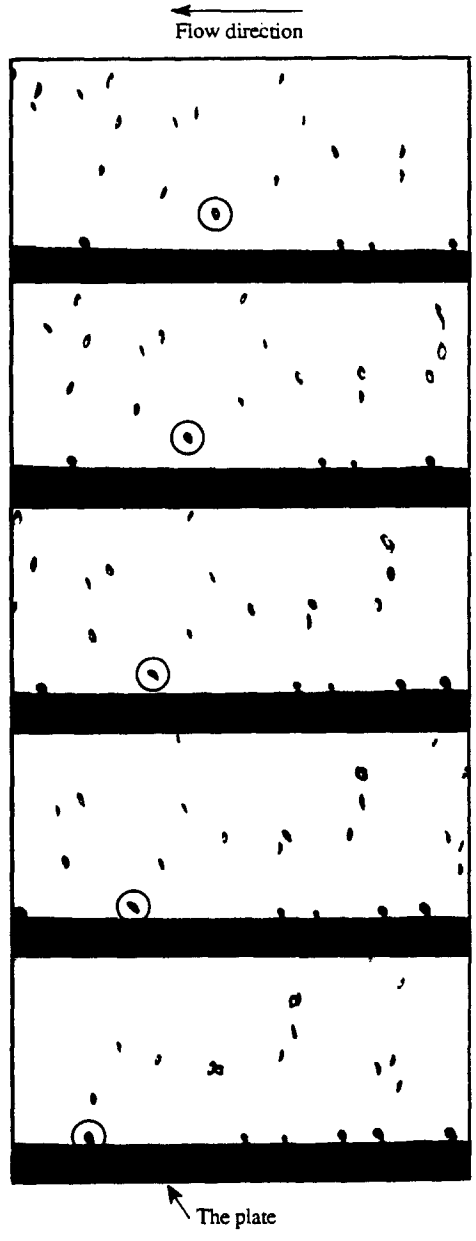

Figure 6. An example of images taken from the high speed video film at different time intervals. $U_{LE} = 0.5$ m/s; $X = 1$ m. Within the circles: a bubble migrating towards the wall (see section 5.1).

quite well, if the friction velocity U_* is taken to be equal to 4.2 cm/s. The latter value differs within 5% from that given by the Preston tube (4.4 cm/s), which is lower than the maximum deviation usually observed in such flows. As a consequence, we conclude that there is no significant pressure gradient along the X-axis (Tennekes & Lumley 1972), and that the low free-stream turbulence (< 1%) generated by the injection grid does not affect the flow on the plate (Hancock & Bradshaw 1983).

4.2. Inlet conditions for the dispersed phase

The void fraction profiles upstream of the flat plate prove to be quite flat as required, except for regions close to the walls (figure 5). It is expected however that the size distribution of the oblate

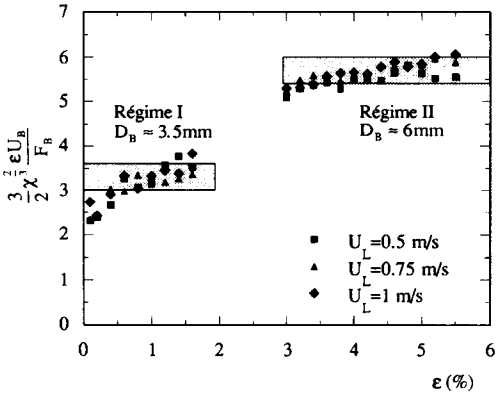

Figure 7. Evolution of the mean equivalent bubbles diameter upstream of the plate.

spheroidal bubbles injected exhibits some non-uniformity since their diameters cannot be controlled in such an experiment. A systematic investigation of the granulometry of a swarm of large millimetric bubbles cannot be performed easily with a standard measuring device. Moreover, image processing techniques, although feasible, are known to be extremely lengthy. As a result, in order to roughly estimate the statistical average of the equivalent diameter of the bubbles and the range of their variation, two complementary simpler methods were used. First, from a careful inspection of the high speed video films made (see figure 6), it was inferred that whatever the liquid velocity, the probability density function for bubble size distribution seemed to peak sharply around a mean equivalent diameter $\bar{D}_B = 3.5$ mm for very low void fractions, while broadening significantly from $D_B = 3$ mm to $D_B = 8$ mm as ϵ increased. In addition, the same technique provided the lower and the upper bounds of the relative velocity of the smaller and larger bubbles

$$17 \text{ cm/s} < U_R < 25 \text{ cm/s} \qquad [3]$$

as well as the average ratio of their major and minor axes, $\chi = 2$. On the other hand, it is known that at a given point for bubbly flow, the incoming frequency of the bubbles F_B may be linked to the void fraction ϵ by a relationship which depends on the bubble geometry (Clark & Turton 1988). For oblate spheroids, which is an extension of the case examined by Herringe & Davis (1976), it may be written under the form:

$$\frac{3}{2}\chi^{\frac{2}{3}}\frac{\epsilon U_B}{F_B} = \bar{D}_B \qquad [4]$$

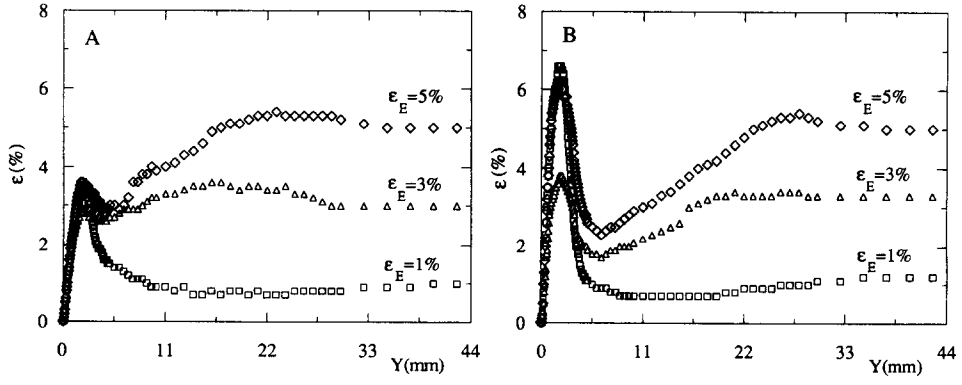

Figure 8. Void fraction profiles at $X = 1$ m. (A) $U_{LE} = 0.5$ m/s; (B) $U_{LE} = 1$ m/s.

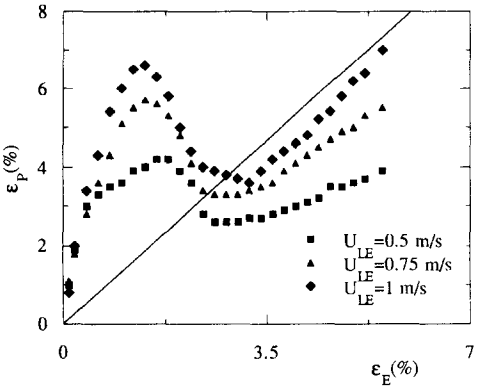

Figure 9. Void fraction peak versus external void fraction at $X = 1$ m.

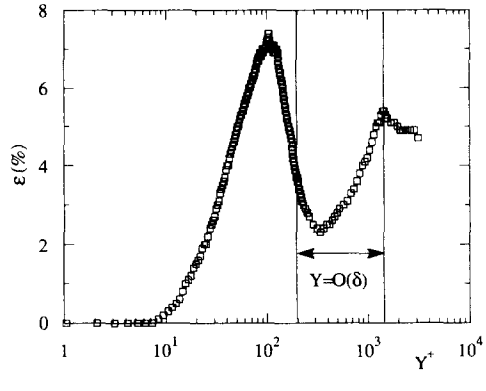

Figure 10. Void fraction profile in inner variable. $X = 1$ m; $U_{LE} = 1$ m/s; $\epsilon_E = 5\%$.

Therefore, if F_B is measured as a function of ϵ at a given value of U_L, say $U_L = 1$ m/s—in which case U_B is approximately constant, $U_B = 1.21$ m/s, in view of [3]—the left hand side of [4] should be a constant if the size distribution were uniform. It is observed from figure 7 that this is not the case and that such a behavior only holds asymptotically at low and higher void fractions. The associated mean diameters $\bar{D}_B$ are respectively $\bar{D}_B = 3.4$ mm and $\bar{D}_B = 5.8$ mm, in agreement with those provided by the visualization. The same trend is observed at all liquid velocities investigated. As a result, it is reasonable to assume that at very low void fractions ($0\% < \epsilon < 1.5\%$) the overwhelming majority of the bubbles are relatively small ($\bar{D}_B = 3.5$ mm) whereas at higher void fractions ($3\% < \epsilon < 5.5\%$), the equivalent diameters of the bubbles range from 3 to 8 mm, most of them being closer to 6 mm. This is consistent with the bubble formation mechanisms: in the first case, bubbles are expected to be produced one by one (discontinuously) at the tip of the injectors as opposed to the break-up of small jets expected at higher void fractions.

5. RESULTS AND DISCUSSION

5.1. Void peaking and void migration at a given section ($X = 1$ m)

Typical void fraction profiles at $X = 1$ m, are shown in figure 8, for two different liquid velocities $U_L = 0.5$ m/s and $U_L = 1$ m/s, and three different upstream void fractions $\epsilon_E = 1, 3, 5\%$. The void fraction exhibits a sharp relative or absolute maximum ϵ_P (see figure 9) at a distance $Y \approx 2$ mm from the wall, very slightly greater than the mean equivalent radius of the smaller bubbles, and asymptotically recovers its free-stream value either monotonously or after going through a minimum. Such a feature is even better brought out when inner variables are used to plot the void fraction profiles, i.e. $Y^+ = YU_*/\nu$ where U_* was determined under two-phase flow conditions from the measurements performed with the flush-mounted hot film (see section 5.3). Indeed, figure 10 clearly shows that there are no bubbles at the wall and that the width of the void deficit region is of the order of the boundary layer thickness, δ. The void peaking phenomenon observed here in a comparatively simple situation is not surprising in view of the findings of a number of authors dealing with upward pipe flows (Serizawa *et al.* 1975; Wang *et al.* 1987; Liu & Bankoff 1990). It is very often attributed to so-called void migration. In view of [4] however, one may wonder whether the sharp increase of ϵ at the wall should be associated with an increase of the bubble frequency F_B and therefore with an actual void migration, and/or with the deceleration of the bubbles which is bound to take place at the wall, let alone the variation of the bubble diameter $\bar{D}_B$.

Table 1. Photographic estimation of the velocity of the bubbles at the wall (U_{BP}) in regime I, showing that $\epsilon_E U_{BE} < \epsilon_P U_{BP}$

U_{LE}(m/s)	ϵ_E(%)	U_{BE}(m/s)	ϵ_P(%)	U_{BP}(m/s)	$\epsilon_E U_{BE}$(cm/s)	$\epsilon_P U_{BP}$(cm/s)
0.50	1.5	0.75	4.2	0.53	1.13	2.23
0.75	1.5	0.96	5.8	0.60	1.44	3.48
1.00	1.5	1.19	6.8	0.74	1.79	5.03

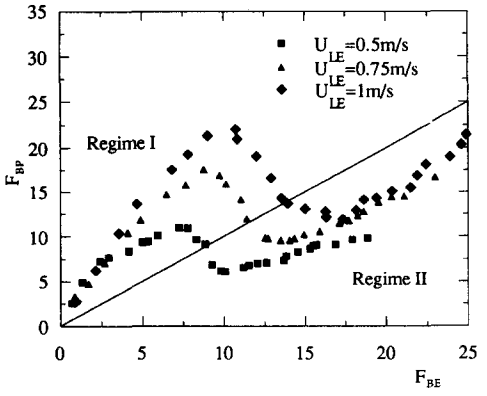

Figure 11. Bubble frequency at the peak location versus the external frequency. $X = 1$ m.

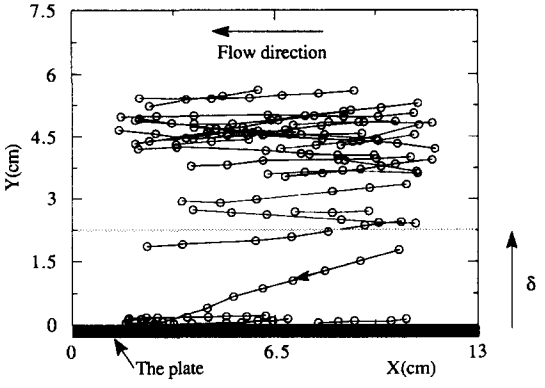

Figure 12. Typical bubbles trajectories within the boundary layer. Image processing by Simöens (1992). Time interval between two consecutive bubble positions: 10 ms. $U_{LE} = 0.75$ m/s; $X = 1$ m.

The influence of the latter phenomenon can be best evaluated at very low void fractions, where the mean diameter of the bubbles $\bar{D}_B$ is approximately constant ($\bar{D}_B \approx 3.5$ mm) as discussed in section 4.2. Under such conditions, the deceleration of the bubbles at the wall, inferred from the video film, although significant, cannot possibly account alone for the observed void peaking, since ϵU_B at the wall ($\epsilon_P U_{BP}$) is systematically greater than in the external flow ($\epsilon_E U_{BE}$) as shown in table 1, meaning that some bubbles are deflected towards the plate. Indeed if they were not, mass conservation for a steady flow would require that

$$\frac{\partial}{\partial X}(\epsilon U_B) = \frac{\partial}{\partial X}(F_B) = 0 \qquad [5]$$

or

$$\epsilon(Y)U_B(Y) = \epsilon_E U_{BE} \text{ or } F_B(Y) = F_{BE} \qquad [6]$$

since the injection (or the gas flow-rate) is crosswise uniform.

Accordingly, it proved necessary, and of course more accurate, to investigate the behavior of the bubble frequency, as provided by the optical probe, rather than the void fraction. Figure 11, which gives the evolution of the bubble frequency at the peak, close to the wall, F_{BP} as a function of its free-stream value F_{BE}, clearly shows that void migration does not systematically occur and is size dependent. Indeed in regime I, the amount of bubbles deflected towards the wall is significant and increases strongly with the liquid velocity. However, no net statistical deflection of the bubbles towards the wall takes place in regime II, which corresponds to relatively high values of the external void fraction. This is consistent with the qualitative conclusions drawn from the inspection of the video film (figure 6) which indicate that a significant number of bubbles migrate or not, depending on the operating conditions. Typical trajectories of the bubbles are shown in figure 12, which have been obtained, applying to one of our vizualisations, an image processing technique developed in our laboratory by Simöens (1992) which is similar to that used by Perkins in the Department of Applied Mathematics and Theoretical Physics of Cambridge University. The same cinematographic evidence also suggests that it is mainly the small bubbles ($\bar{D}_B \approx 3.5$ mm) which migrate to and remain at the wall, whereas the larger ones are hardly deflected, and if so bounce off. As a consequence, it is obvious that the discrimination between the migrating and non-migrating populations of bubbles should not be made in terms of the external void fraction, which only determines the significance of the hydrodynamic mutual interactions, but also in terms of their mean size. That the diameter of the bubbles should play such an important role is not totally unexpected. Indeed, although still not clearly understood, the deflection of a given bubble in a highly sheared turbulent flow, can reasonably be associated with the following mechanisms

(a) deformation of the bubble and modification of its wake as affected by the velocity gradient,
(b) interaction between the bubble and its wake with the surrounding turbulent eddies.

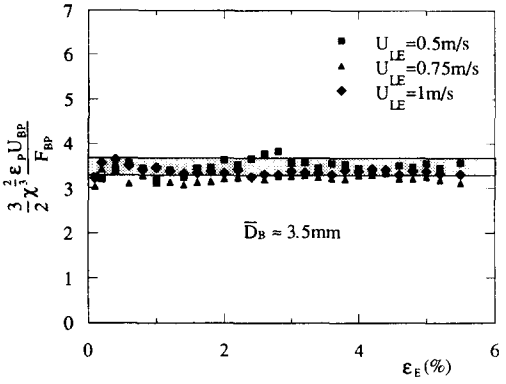

Figure 13. Mean equivalent bubbles diameter at the wall. $X = 1$ m.

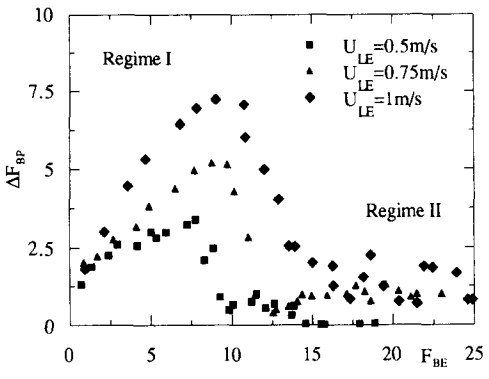

Figure 14. Increase of the bubble peak frequency between $X = 0.2$ and $X = 1$ m. $\Delta F_{BP} = (F_{BP})_{X=1\,m} - (F_{BP})_{X=0.2\,m}$.

Both phenomena are partly controlled by the diameter $\bar{D}_B$.

In order to identify which bubbles do migrate to the wall, it is useful to plot $\bar{D}_B$ as calculated from [4] using the measured values of ϵ_P, F_{BP}, U_{BP}. It is seen in figure 13 that the average equivalent diameter $\bar{D}_B$ is approximately constant ($\bar{D}_B \approx 3.5$ mm) whatever ϵ_E for all external liquid velocities, meaning that the majority of the bubbles at the surface are indeed the smaller ones. Here the ratio of major and minor axes (χ) was taken to be equal to 1, since close to the wall, the bubbles are roughly spherical. The above experimental findings support the idea that there exists a "critical range of diameters", around $\bar{D}_B \approx 3.5$ mm in our experiment, below which bubbles may undergo migration and above which no migration is expected. Similar conclusions have been reached by Serizawa *et al.* (1988), Monji & Matsui (1991), Liu (1993), Zun *et al.* (1992), in different contexts. In view of the above, regime II of figure 11, where no net statistical migration of the bubbles takes place, should be thought of as a domain of the operating plane where a significant fraction of the population of bubbles have large diameters, according to our injection system (see section 4.2), rather than a region where void fractions are high.

5.2. *Streamwise behavior*

The analysis of the streamwise behavior of the void peaking phenomena supports the view developed in the previous section that deflection of the bubbles towards the wall does take place but mainly affects the smaller bubbles. Indeed, figure 14 clearly shows that between station $X = 0.2$ m and $X = 1$ m, the observed increase in the peak frequency, $\Delta F_{BP} = (F_{BP})_{X=1\,m} - (F_{BP})_{X=0.2\,m}$, is only very significant at low values of the void fraction, when the injected bubbles are rather small (see section 4.2).

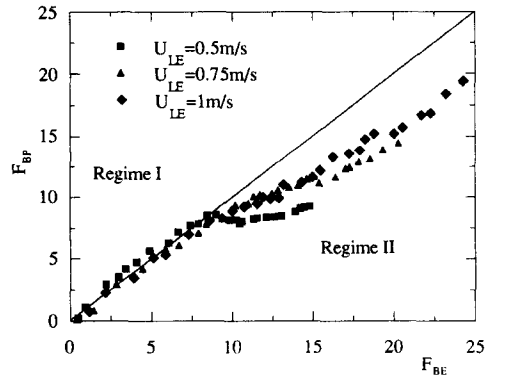

Figure 15. Bubble frequency at the peak location versus the external frequency. $X = 0.07$ m.

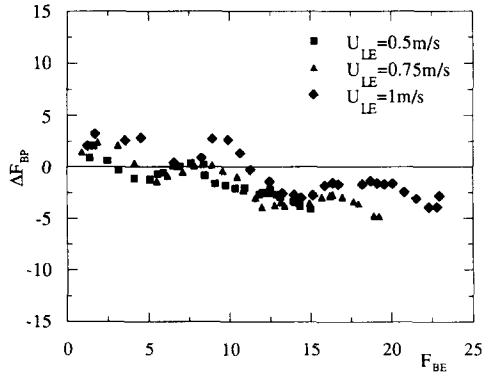

Figure 16. Saturation of the bubble peak frequency between $X = 1$ and $X = 1.5$ m. $\Delta F_{BP} = (F_{BP})_{X=1.5\,m} - (F_{BP})_{X=1\,m}$.

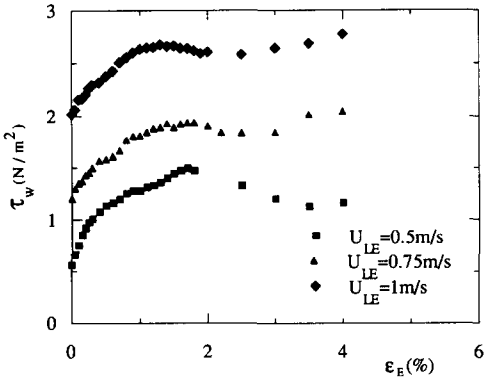

Figure 17. Variation of the mean wall shear stress as a function of the external void fraction. $X = 1$ m.

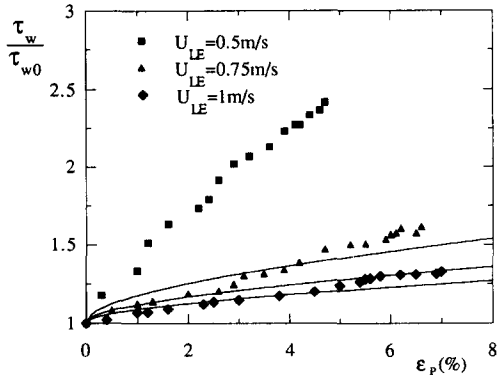

Figure 18. Ratio of the wall shear stress in bubbly and single-phase flows versus the peak of void fraction. $X = 1$ m, —— Marié's model (1987).

On the other hand, the study of the initial behavior—i.e. at $X = 0.07$ m—of the bubbles at the walls (figure 15) shows that almost no net statistical migration has occurred, ($F_{BP} = F_{BE}$), which is reasonable, at least for the low values of F_{BE} when the majority of the bubbles are known to be small. This however does not hold for large values of F_{BE} ($F_{BE} > 10$), where $F_{BP} < F_{BE}$, suggesting that the bigger bubbles produced under such conditions (see section 4.2) are carried away from the wall.

Finally, it is worth noting (figure 16) that some kind of saturation of the layer of bubbles at the wall seems to take place further downstream ($X = 1.5$ m), since there is hardly any increase in the peak bubble frequency between $X = 1$ m and $X = 1.5$ m: $\Delta F_{BP} = (F_{BP})_{X=1.5\text{m}} - (F_{BP})_{X=1\text{m}} \approx 0$

5.3. Wall shear stress and velocity profiles

From the data displayed in figure 17, one notes that the evolution of the wall shear stress versus the external void fraction is similar to that exhibited by the bubble frequency at the surface. This is evidence that the momentum transfer near the wall strongly depends on the void peaking phenomenon. Such a dependence is even more obvious when the data are directly plotted as a function of the peak value ϵ_P (figure 18). Indeed, in this form, we see that the skin friction increases with the amplitude of the maximum and that, for constant ϵ_P, the increase is greater for low values of the external velocity. Such a behavior was explained by Marié (1987), who proposed a simple physical model accounting for the trends reported in the literature. This model assumes that the flow is upward vertical, steady and fully developed, and that the effect of the dispersed phase on the velocity profile near the wall is comparable with the action of a grid-generated turbulence on a single-phase turbulent boundary layer: the universal logarithmic law of the wall is therefore supposed to hold with its usual slope and additive constant, whereas the wake function is strongly

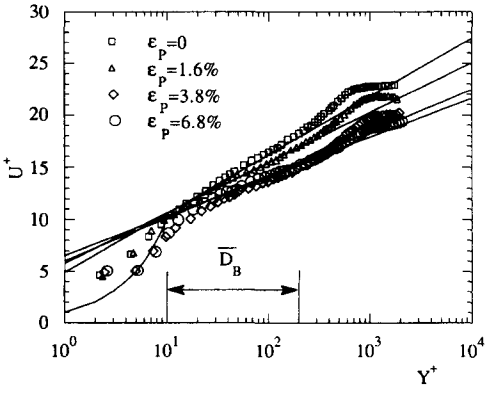

Figure 19. Logarithmic velocity profiles in bubbly flow. $X = 1$ m; $U_{LE} = 1$ m/s.

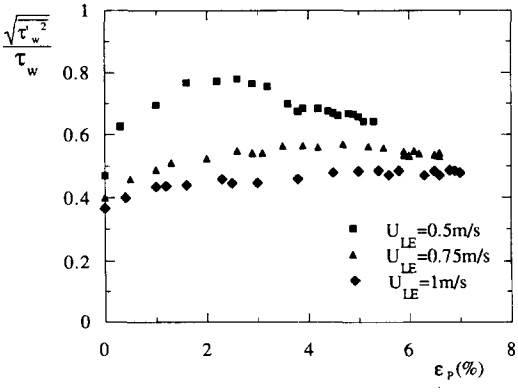

Figure 20. Intensity of the wall shear stress fluctuations versus the peak of void fraction.

Table 2. Coefficients of the law of the wall as a function of the void fraction

U_{LE}(m/s)	ϵ_E(%)	ϵ_P(%)	K	C
1	0	0	0.41	4.9
1	0.2	1.6	0.48	5.8
1	0.5	3.8	0.56	6
1	1.5	6.8	0.61	6.5

depressed by the additional turbulence caused by the bubbles. The correlations thus obtained, which only require the knowledge of the turbulent intensity and the integral length scale in the wall region are shown to compare qualitatively well with the present data, but not quantitatively (figure 18). This suggests that other mechanisms are probably involved in the friction modification.

Although the structure of the boundary layer is currently under investigation, a few velocity profiles have already been obtained with a miniature conical hot film (figure 19) using the signal processing technique described in Moursali (1993), which shows that a logarithmic law of the wall actually holds for void fraction peaks as large as 7% and that a wake depression also occurs. But contrary to what was assumed in the model, the Karman constant proves to significantly increase with the void fraction (see table 2), meaning that the mixing length is larger when there are bubbles sliding at the wall. Under such conditions, the wake depression is probably the result of two combined effects: the modification of the turbulence in the outer layer and the increase of the Karman constant. The latter analysis has of course to be confirmed by more detailed experimental information.

Finally, the relative wall shear stress fluctuations (figure 20) are shown to increase with ϵ_P, which is consistent with the fact that the bubbles sliding along the surface generate significant velocity perturbations, even in the viscous sublayer. It should be noted that the very high level of fluctuation observed (80%) in fact corresponds to relative voltage fluctuations which are sufficiently small (5%) to fulfil the conditions discussed in section 1.

6. CONCLUSION

It has been shown that the now familiar wall void peaking phenomenon, which is partly due to the deceleration of the bubbles close to the wall, also involves an actual migration of the bubbles from the external flow to the walls which is however not systematic since it is strongly size dependent. On the other hand the wall shear stress proves to increase significantly with the amplitude of the void peak. Moreover, the mean liquid velocity profiles are shown to follow a modified logarithmic law.

Finally it is worth noting that the void fraction data obtained here have been used to qualify a two-fluid model numerical code, recently developed in our group (see Lance & Lopez de Bertodano 1992).

Acknowledgements—The authors wish to acknowledge Dr S. Simöens' contribution to the processing of the flow visualizations and Dr R. Perkins (Department of Applied Mathematics and Theoretical Physics of Cambridge University) as well as Professors I. Zun (Ljubljana) and M. Lance (Université Claude Bernard) for fruitful and stimulating discussions.

The present work was partially funded by the Direction des Recherches, Etudes et Techniques, Centre National de la Recherche Scientifique, Ministère de la Recherche et de l'Espace, and Ministère de l'Education Nationale (Alliance Program).

Special thanks are expressed by Dr J. L. Marié and E. Moursali to Professor M. Lance for the very efficient role he played in finding the extra financial support to complete the present part of the research program.

REFERENCES

BELLHOUSE, B. J. & SCHULTZ, D. L. 1966 Determination of mean and dynamic skin friction, separation and transition in low-speed flow with a thin-film heated element. *J. Fluid Mech.* **24,** 379–400.

CLARK, N. N. & TURTON, R. 1988 Chord length distributions related to bubble size distributions in multiphase flows. *Int. J. Multiphase Flow* **14,** 413–424.

HANCOCK, P. E. & BRADSHAW, P. 1983 The effect of free-stream turbulence on turbulent boundary layers. *ASME J. Fluids Engng* **105,** 284–289.

HERRINGE, R. A. & DAVIS, M. R. 1976 Structural development of gas–liquid mixture flows. *J. Fluid Mech.* **73,** 97–123.

LANCE, M. & BATAILLE, J. 1991 Turbulence in the liquid phase of a uniform bubbly air–water flow. *J. Fluid Mech.* **222,** 95–118.

LANCE, M., MARIÉ, J. L. & BATAILLE, J. 1991 Homogeneous turbulence in bubbly flows. *ASME J. Fluids Engng* **113,** 295–300.

LANCE, M. & LOPEZ DE BERTODANO, M. 1992 Phase distribution phenomena and wall effects in bubbly two-phase flows. Presented at the *3rd International Workshop on Two-phase Flow Fundamentals*, Imperial College, London.

LIU, T. J. & BANKOFF, S. G. 1990 Structure of air–water bubbly flow in a vertical pipe: II Void fraction, bubble velocity and bubble size distributions. *Int. Symp. on Gas–Liquid Two-phase Flows, ASME Winter Annual Meeting*, Dallas, TX.

LIU, T. J. 1993 Bubble size and entrance length effects on void development in a vertical channel. *Int. J. Multiphase Flow* **19,** 99–113.

MARIÉ, J. L. & LANCE, M. 1983 Turbulence measurements in two-phase bubbly flows using laser Doppler anemometry. In *Proc. of UTAM Symposium on Measuring Techniques in Gas–Liquid Two-phase Flows* (Edited by DELHAYE, J. M. & COGNET, G.), pp. 141–148, Springer-Verlag, Berlin.

MARIÉ, J. L. 1987 Modelling of the skin friction and heat transfer in turbulent two-component bubbly flows in pipes. *Int. J. Multiphase Flow* **13,** 309–325.

MICHIYOSHI, I. & SERIZAWA, A. 1984 Turbulence in two-phase bubbly flows. Presented at *Japan/U.S. Seminar on Two-phase Flow Dynamics*, Lake Placid, NY.

MONJI, H. & MATSUI, G. 1991 Effect of bubble size on structure of vertical bubble flow. In *Proc. of the Int. Conf. on Multiphase Flows*, pp. 449–452, Tsukuba.

MOURSALI, E. 1993 Etude expérimentale d'une couche limite eau-air à bulles se développant sur une plaque plane verticale. Ph.D. thesis, Ecole Centrale de Lyon, Ecully, France.

SANDBORN, V. A. 1979 Evaluation of time-dependent surface shear stress in turbulent flows, ASME paper 79-WA/FE-17.

SCHLICHTING, H. 1968 *Boundary Layer Theory*, 6th edn. McGraw–Hill, New York.

SERIZAWA, A., KATAOKA, I. & MICHIYOSHI, I. 1975 Turbulence structure of air–water bubbly flows: Part II, Local properties. *Int. J. Multiphase Flow* **2,** 235–246.

SERIZAWA, A., KATAOKA, I., ZUN, I. & MICHIYOSHI, I. 1988 Bubble size effect on phase distribution. In *Proc. of the Japan/U.S. Seminar on Two-phase Flow Dynamics*, pp. 15–20, Ohtsu, Japan.

SIMÖENS, S. 1992 Applications de l'analyse d'images à des phénomènes de mélange et de dispersion turbulents. Ph.D. thesis, Ecole Centrale de Lyon, Ecully, France.

SOUHAR, M. 1989 Some turbulence quantities and energy spectra in the wall region in bubble flow. *Phys. Fluids A* **1,** 1558–1565.

TENNEKES, H. & LUMLEY, J. L. 1972 *A First Course in Turbulence*, pp. 146–196. MIT Press, Cambridge, MA.

WANG, S. K., LEE, S. J., JONES, O. C. & LAHEY, R. T. 1987 3D Turbulence structure and phase distribution measurements in bubbly two-phase flows. *Int. J. Multiphase Flow* **13,** 327–343.

ZUN, I., KLJENAK, I. & SERIZAWA, A. 1992 Bubble coalescence and transition from wall void peaking to core void peaking in turbulent bubbly flow. In *Dynamics of Two-phase Flows* (Edited by JONES, O. C. & MICHIYOSHI, I.), pp. 233–249. Boca Raton, FL.